Concepts for Integrating Plastic Anisotropy into Metal Forming Simulations

By *Dierk Raabe*,* *Peter Klose*, *Bernhard Engl*, *Klaus-Peter Imlau*, *Frank Friedel*, and *Franz Roters*

Modern metal forming and crash simulations are usually based on the finite element method. Aims of such simulations are typically the prediction of the material shape, failure, and mechanical properties during deformation. Further goals lie in the computer assisted lay-out of manufacturing tools used for intricate processing steps. Any such simulation requires that the material under investigation is specified in terms of its respective constitutive behavior. Modern finite element simulations typically use three sets of material input data, covering hardening, forming limits, and anisotropy. The current article is about the latter aspect. It reviews different empirical and physically based concepts for the integration of the elastic-plastic anisotropy into metal forming finite element simulations. Particular pronunciation is placed on the discussion of the crystallographic anisotropy of polycrystalline material rather than on aspects associated with topological or morphological microstructure anisotropy. The reviewed anisotropy concepts are empirical yield surface approximations, yield surface formulations based on crystallographic homogenization theory, combinations of finite element and homogenization approaches, the crystal plasticity finite element method, and the recently introduced texture component crystal plasticity finite element method. The paper presents the basic physical approaches behind the different methods and discusses engineering aspects such as scalability, flexibility, and texture update in the course of a forming simulation.

1. Introduction

The advance of modern well-tailored and optimized materials nowadays provides a huge and steadily-growing application spectrum to customers of formed products. Well established examples are the introduction of high-strength multi-phase steels or 6xxx series aluminum alloys for the automotive industry. The high demands with respect to mechanical properties and surface appearance faced by these materials in the course of metal forming increasingly requires adequate quantitative characterization measures to build a bridge between producers and product designers.

Modern approaches for conducting simulations of plastic deformation are usually based on solving large sets of differential equations associated with a well posed forming problem by use of non-linear finite element methods. Primary objectives of such simulations are the prediction of the material shape after forming, in particular the thickness distribution; the minimization of material failure in conjunction with the optimization of material flow during forming; and the cal-

[*] *Prof. D. Raabe, Dr. F. Roters*
Max-Planck-Institut für Eisenforschung GmbH
Abteilung für Mikrostrukturphysik und Umformtechnik
Max-Planck-Str. 1, 40237 Düsseldorf (Germany)
E-mail: raabe@mpie.de
Dr. P. Klose, Dr. B. Engl, Dr. K.-P. Imlau, Dr. F. Friedel
Research & Development, Quality Engineering, and Materials Testing
Thyssen Krupp Stahl AG, Kaiser-Wilhelm-Strasse 100,
D-47166 Duisburg (Germany)

  1438-1656/02/0404-0169 $ 17.50+.50/0

culation of the final mechanical properties of the formed sample. Further related essential applications are in the fields of optimizing tool designs, predicting pressing forces, and simulating the final surface appearance of the part. The latter aspect involves both, macroscopic (e.g., wrinkling) as well as microstructural (e.g., ridging, orange peel) mechanisms for changes in surface quality during forming.

Rendering continuum-type metal forming simulations scientifically sound, predictive at the microstructure scale, in good accord with experiment, and at the same time economically rewarding requires that the involved materials are properly specified in terms of their respective constitutive behavior. For this purpose modern finite element simulations typically employ three sets of material input data, covering hardening, forming limits, and anisotropy (Fig. 1). The current article deals with the latter aspect. It reviews both, empirical and physically based concepts for the integration of the elastic-plastic anisotropy into metal forming finite element simulations. Particular pronunciation is placed on the discussion of the crystallographic anisotropy of polycrystalline material rather than on aspects associated with topological or morphological microstructure anisotropy. The various anisotropy concepts which will be reviewed in the following are empirical yield surface approximations, yield surface formulations based on crystallographic homogenization theory, combinations of finite element and homogenization approaches, the crystal plasticity finite element method, and the recently introduced texture component crystal plasticity finite element method.

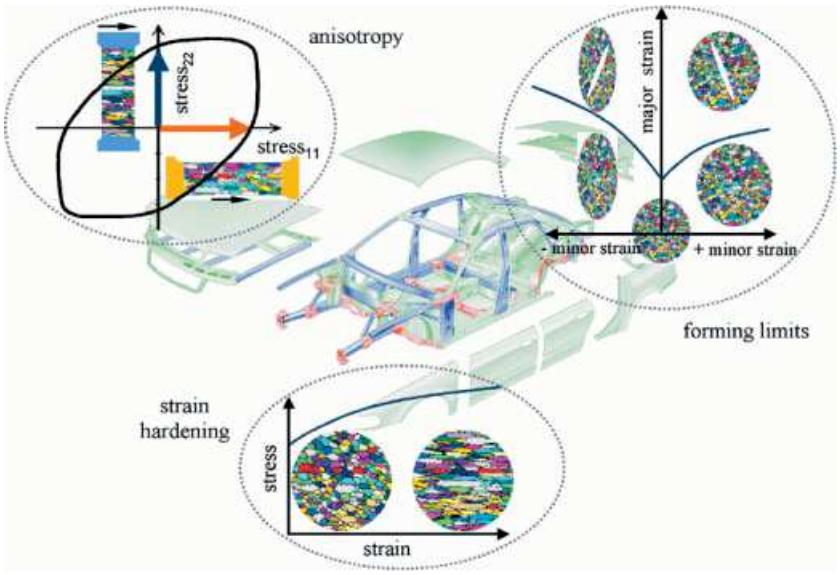

Fig. 1. Modern finite element approaches which aim at simulating realistic metal forming operations typically require three sets of material input data, namely, the strain hardening curve, a forming limit diagram, and information about the crystallographic (and morphological) anisotropy. The article focuses on concepts for integrating elastic-plastic anisotropy.

By providing a survey on the advantages and disadvantages of the various anisotropy concepts the article takes an effort to present both, the present state of the art in the industrial practice as well as advanced approaches which allow the user to include more of the physics associated with crystalline anisotropy. The present state in anisotropy engineering is naturally different between industrial applications and basic science. The use of empirical or semi-empirical polynomials for yield surface approximations is the standard procedure in the industrial practice whereas the various crystal plasticity finite element methods gradually become a standard in the basic materials sciences. The importance of empirical approaches in the industrial practice is due to the fact that they provide short computation times, allow for simple mechanical input data, and are flexible with respect to additional fit points obtained by texture information. An important weakness of empirical approaches lies in the absence of texture update. The prevalence of the crystal plasticity finite element method in basic research is due to its physical basis and the incorporation of texture changes. The major drawback of the crystal plasticity approaches are the long calculation times which presently exceed those obtained by use of the yield surface by a factor of 50–100. An improvement in speed of the crystal plasticity methods is attained by the recent introduction of the texture component crystal plasticity finite element method which exceeds the computation times of yield surface calculations only by a factor of 15–25.

The paper has the following plan: First, we give a brief introduction to the physical origin of elastic-plastic crystallographic anisotropy. Second, we present the basic approaches behind the different anisotropy concepts and discuss aspects such as scalability, flexibility, and texture update in the course of forming simulation.

2. From Scalar to Tensorial Materials Engineering

The yield surface represents the generalization of the yield point from uniaxial tensile testing to general stress states. Expanding the yield point into a closed yield surface is only required if the material under inspection shows elastic-plastic anisotropy, i.e., if it deforms differently in different directions. However, such behavior is the rule and not the exception in real materials. Polycrystals with random and thus quasi-isotropic behavior do practically not occur in sheet metal forming operations. Strong crystalline anisotropy is typically encountered in many engineering materials such as alloys based on iron, aluminum, copper, magnesium and titanium.

The physical nature of elastic-plastic anisotropy in metals is the crystalline arrangement of the atoms. Metallic matter usually occurs in polycrystalline form where each grain has a different crystallographic orientation, shape and volume frac-

ADVANCED ENGINEERING MATERIALS

tion. The distribution of the orientations in a polycrystalline aggregate is referred to as crystallographic texture. The anisotropy of the elastic tensor and the discrete nature of crystallographic slip along densely packed lattice directions on preferred crystal planes also entails a highly anisotropic integral response of such polycrystalline specimens during mechanical loading. While the elastic-plastic deformation of a single crystal and bicrystals as a function of their orientation can nowadays be well predicted, plasticity of polycrystalline matter is less well understood. This is essentially due to the intricate elastic-plastic interactions occurring during co-deformation among the highly anisotropic individual crystals. This interaction leads to strong heterogeneity in terms of strain, stress, and crystal orientation. Another difficulty in tackling the anisotropy of polycrystalline matter lies in the fact that the crystals rotate during forming, owing to the skew symmetric portion of the displacement gradients created by crystal slip. This means that texture and anisotropy gradually change during forming, even under constant strain path conditions. In this context it must be underlined that crystallographic orientation changes are principally non-reversible owing to the orientation sensitivity of strain path changes and the orientation dependence of strain hardening (Not only the beginning of plastic yield but also further strain hardening is a tensorial, i.e., highly anisotropic orientation dependent problem.) This means that - even in the case of very simple strain paths - mechanics and texture should wherever possible be integrated into the simulation concept due to the strong non-linearity of the problem. Artificial separation of the two aspects (continuum mechanics, crystal plasticity mechanics) may entail severe misinterpretations, particularly in the case of strain path changes.

These various aspects which show the complexity of texture and anisotropy and their evolution during forming underline that for an engineering purpose one major aim of polycrystal research must lie in identifying adequate measures for mapping crystallographic anisotropy into classical mathematical methods for predicting large strain plastic deformation. The second even more challenging aim lies in developing methods for predicting also the change of crystal anisotropy during forming on a sound physical basis.

3. The Physical Origin of Crystalline Elastic-Plastic Anisotropy

3.1. Elastic Anisotropy

The elastic anisotropy of crystalline matter departs from the directionality of the electronic bond and the resulting crystal lattice structure. For small deviations of the atoms from their equilibrium positions the reversible elastic response to loads can be approximated by a linear relationship which is referred to as Hooke's law. In this framework the linear elastic constants can be derived as the components of the second derivative of the electronic potential. The elastic constants can be written in the form of a fourth-rank elastic stiffness tensor C_{ijkl} or in the form of a fourth-rank elastic compliance tensor S_{ijkl} According to

$$\sigma_{ij} = C_{ijkl}\,\varepsilon_{kl} \qquad \varepsilon_{ij} = S_{ijkl}\,\sigma_{kl} \tag{1}$$

Symmetry relations and thermodynamic considerations reduce the 81 elastic constants to a set of 3 independent numbers (C_{1111}, C_{1122}, C_{2323}) (Corresponding to (C_{11}, C_{12}, C_{44}) in reduced matrix notation)in the case of cubic crystal symmetry (e.g., Al, Fe, Cu) and to a set of five independent numbers (C_{1111}, C_{1122}, C_{1133}, C_{3333}, C_{2323}) (Corresponding to (C_{11}, C_{12}, C_{13}, C_{33}, C_{44}) in reduced matrix notation) in the case of hexagonal crystal symmetry (e.g., Ti, Mg, Zn). The deviation from elastic isotropy can for cubic crystals be quantified by the so called Zener anisotropy ratio

$$A = \frac{2\,C_{2323}}{C_{1111} - C_{1122}} \tag{2}$$

While aluminum has a relatively low elastic anisotropy with A = 1.215, iron has a larger Zener ratio of A = 2.346. Of all cubic metals tungsten has the lowest deviation from isotropy with a Zener ratio of $A \approx 1$ and lithium the largest with A = 9.34.

3.2. Plastic Anisotropy

The plastic anisotropy of crystalline matter also departs from the directionality of the electronic bond and the resulting crystal lattice structure. Both aspects determine which slip planes and which translation vectors (Burgers vectors) serve for the motion of lattice dislocations or the activation of plastically relevant athermal transformations. The main consequence of this anisotropy in the present context is that metals are deformed in a discrete rather than in a continuum fashion rendering plasticity an intrinsically anisotropic property of metals. Assuming that the normalized Burgers vectors b_j and the normalized slip plane normals n_i of the s different slip systems available in a particular crystal lattice are known, their orientation factors m_{ij} can be readily formulated as dyadic products according to

$$m_{ij}^{s} = n_i^{s}\, b_i^{s} \tag{3}$$

with its symmetric portion being

$$m_{ij}^{\mathrm{sym},s} = \frac{1}{2}\left(n_i^{s} b_j^{s} + n_j^{s} b_i^{s}\right) \quad \textit{(crystal coordinates)} \tag{4}$$

when given in crystal coordinates. One must note that all slip vectors used in the equations are normalized. Transforming the latter equation into the sample coordinate system (Fig. 2) leads to

$$m_{kl}^{\mathrm{sym},s} = \frac{1}{2}\left(a_{ki} n_i^{s}\, a_{lj} b_j^{s} + a_{lj} n_j^{s}\, a_{ki} b_i^{s}\right) \quad \textit{(sample coordinates)} \tag{5}$$

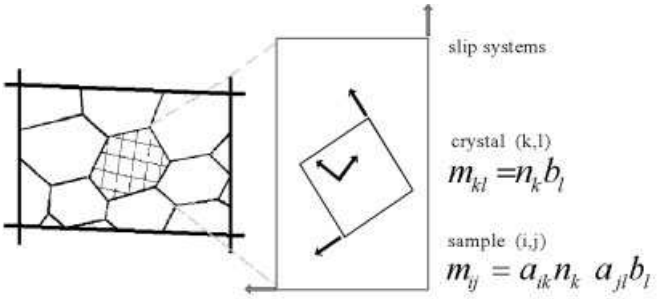

Fig. 2. The plastic anisotropy of crystalline matter departs from the directionality of the electronic bond and the resulting crystal lattice structure. Both aspects determine the slip planes and translation vectors (Burgers vectors) on which lattice dislocations move during plastic deformation. The diagram shows the different coordinate system and the resulting geometrical transformation operations one has to consider in this context.

where a_{ki} and a_{lj} are the transformation matrices between the crystal coordinate system and the sample coordinate system. Using these s different orientation factors $m_{kl}^{\mathrm{sym},s}$ of the s different available slip systems for the transformation of an external load into the slip geometry provides a simple kinematic formulation for the yield surface of a single crystal.

$$\begin{aligned} m_{kl}^{\mathrm{sym},s}\,\sigma_{kl} &= \tau_{\mathrm{crit},+}^{s,\,\mathrm{active}} \\ m_{kl}^{\mathrm{sym},s}\,\sigma_{kl} &= \tau_{\mathrm{crit},-}^{s,\,\mathrm{active}} \end{aligned} \tag{6}$$

for the *active* slip systems, and

$$\begin{aligned} m_{kl}^{\mathrm{sym},s}\;\;\sigma_{kl} &< \tau_{\mathrm{crit},+}^{s,\,\mathrm{nonactive}} \\ m_{kl}^{\mathrm{sym},s}\;\;\sigma_{kl} &< \tau_{\mathrm{crit},-}^{s,\,\mathrm{nonactive}} \end{aligned} \tag{7}$$

for the *non-active* slip systems (Fig. 3). One must note that the Einstein summation rule applies in all equations in case not stated otherwise. While the slip dyads of cubic systems typically contain <111> and <110> vectors (fcc, bcc) as well as <111> and <112> vectors (bcc), hexagonal materials deform by slip on basal, prismatic, and pyramidal systems depending on their cell aspect ratio.

Most points on the single crystal yield surface describe single-slip conditions. In the graphical representation of the yield surface single-slip generally takes place when the stress tensor (in vector transformation notation, using the tensor-vector transformation rule see Equation 8)

$$\sigma_{\lambda}^{\mathrm{T}} = \left\{ \frac{1}{\sqrt{6}}(2\sigma_{33} - \sigma_{11} - \sigma_{22}), \frac{1}{\sqrt{2}}(\sigma_{22} - \sigma_{11}), \sqrt{2}\sigma_{23}, \sqrt{2}\sigma_{13}, \sqrt{2}\sigma_{12} \right\} \tag{8}$$

points at a hyperplane rather than a hyperconus (Fig. 4). Note that the cubes placed in Figure 4 indicate the changing orientation of the external reference system, i.e., of the stress state. Polyslip conditions, as usually required for polycrystal deformation owing to the satisfaction of strain rate compatibility among the grains, are characterized by hyperconus coordinates of the stress state (Fig. 5). The conus positions for the stress can be calculated using a conventional homogenization approach, for instance Taylor-Bishop-Hill theory (indicated by δ^{TBH} in Figure 5). The corresponding multislip positions of the stress tensor, satisfying an externally imposed strain rate,

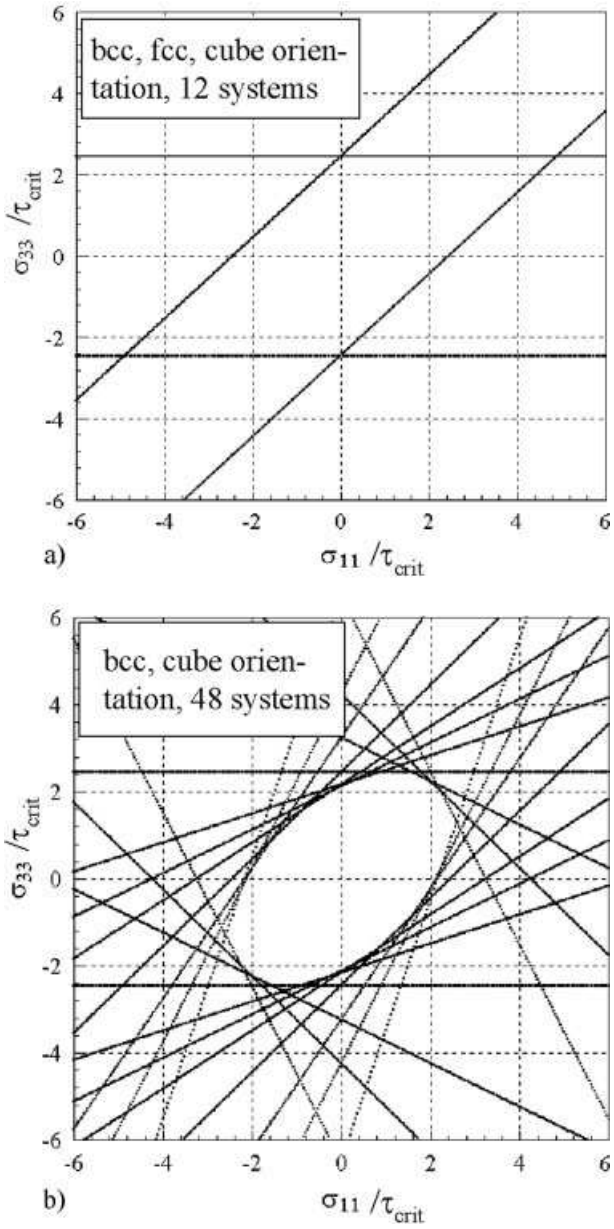

Fig. 3. A simple Schmid-type formulation considering the different orientation factors of all available slip systems which essentially transforms an external load into shear stresses acting on the slip systems provides a kinematic formulation for the yield surface of a single crystal. The yield surface shown in the upper figure (a) was derived using the 12 {110}<111> slip systems. The yield surface shown in the lower figure (b) was derived using the 12 {110}<111>, 12 {112}<111>, and 24 {123}<111> slip systems (body centered cubic). The figure indicates that body centered cubic alloys therefore behave plastically principally different from face centered cubic alloys.

are then denoted as Taylor positions. It must be noted in this context that the Taylor factor generally takes the form of a stress shape tensor for the crystal yield surface rather than that of a factor owing to its dependence on the strain rate tensor. Its magnitude for a given strain rate determines the kinematic size of the yield surface in the corresponding stress direction characterizing the correct polyslip hyperconus and thus the kinematic portion of the corresponding stress state. The symbols $D^{s=1}$ and $D^{s=2}$ in Figure 5 indicate the single slip strain states from slip systems 1 and 2. Using these two slip

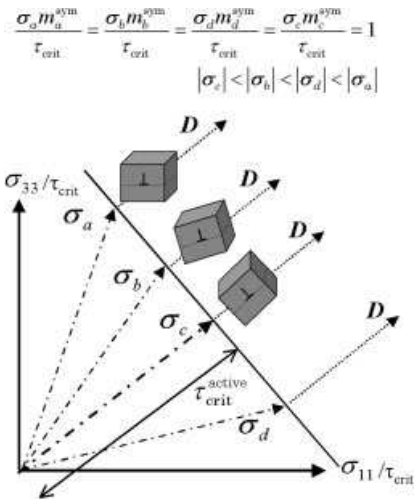

Fig. 4. Most points on the single crystal yield surface describe single-slip conditions. In the graphical representation of the yield surface single-slip generally takes place when the stress state (here given in vector notation) points at a hyperplane rather than a hyperconus. The strain rate tensor is indicated by D and m is the Schmid factor, i.e., the dyadic product of the slip elements. The small cubes placed in the figure indicate the changing relative orientation between the external reference system and the crystal coordinate system.

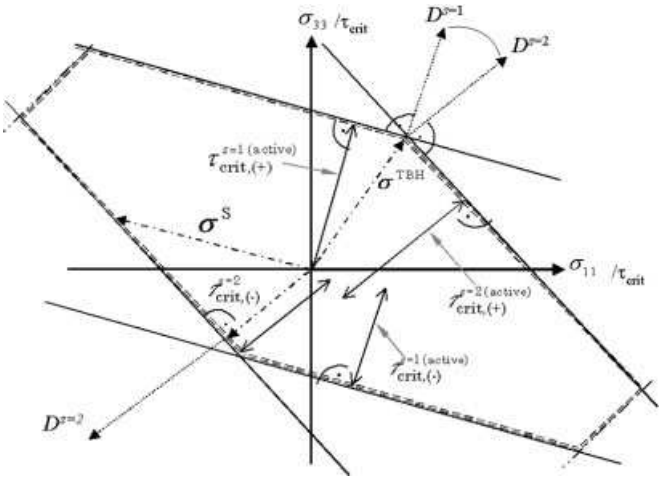

Fig. 5. Polycrystal deformation requires polyslip conditions in order to satisfy strain rate compatibility among the grains. Polyslip states are crystallographically characterized by hyperconus coordinates of the stress state. The conus positions for the stress can be calculated using a conventional homogenization approach, for instance Taylor-Bishop-Hill theory (indicated by δ^{TBH}). The symbols $D^{s=1}$ and $D^{s=2}$ indicate the single slip strain states from slip systems 1 and 2. Using these two slip systems allows one to realize any strain rate state in the respective conus by a linear combination of $D^{s=1}$ and $D^{s=2}$.

systems allows one to realize any strain rate state in the respective conus by a linear combination of $D^{s=1}$ and $D^{s=2}$. For cubic crystals the yield surface reveals 4 classes of Taylor states for polyslip and one for single slip. These yield states are referred to as

penta slip state (5 active slip systems) : ${}^5M_{pq}^i$ (fcc, bcc (reduced): $i = 56$)
tetra slip (4 active slip systems): ${}^4M_{pq}^j$ (fcc, bcc (reduced): $j = 108$)
tri slip (3 active slip systems): ${}^3M_{pq}^k$ (fcc, bcc (reduced): $k = 135$) (9)
bi slip (2 active slip systems): ${}^2M_{pq}^l$ (fcc, bcc (reduced): $l = 66$)
single slip (1 active slip system): ${}^2M_{pq}^n$ (fcc, bcc (reduced): $n = 24$)

where *fcc* denotes *face centered cubic* and *bcc* denotes *body centered cubic* crystal structure. The term *reduced* indicates that only the first 12 {111}<110> bcc slip systems have been considered here. The number at the end of each row gives the number of different conus cases (and single slip cases) for the respective Taylor state. The total Taylor stress state for a polycrystalline aggregate can for a given external strain rate state then be integrated as a volume weighted sum of all Taylor tensors derived separately for each grain for this boundary condition (Fig. 6).

4. Empirical Approximations of the Yield Surface

The first empirical mathematical description of an anisotropic plastic yield surface was suggested in 1928 by von Mises in the form of a quadratic function.[1] This approach which was originally designed to empirically approximate the plastic anisotropy of single crystals was in 1948 rendered by Hill[2] into a generalized form using the Huber-Mises-Hencky approach (Fig. 7a). In Hill's form the yield surface amounts to

$$f(\sigma_{ij}) = \left(F(\sigma_{22}-\sigma_{33})^2 + G(\sigma_{33}-\sigma_{11})^2 + H(\sigma_{11}-\sigma_{22})^2 + 2L\sigma_{23}^2 + 2M\sigma_{13}^2 + 2N\sigma_{12}^2\right)^{1/2} \quad (10)$$

where F, G, H, L, M, and N are the anisotropy coefficients. The above equation can be rewritten as

$$f(S_{ij}) = \left((G+H)S_{11}^2 + (F+H)S_{22}^2 + (F+G)S_{33}^2 - 2HS_{11}S_{22} - 2GS_{11}S_{33} - 2FS_{22}S_{33} + 2LS_{23}^2 + 2MS_{13}^2 + 2NS_{12}^2\right)^{1/2} \quad (11)$$

where S_{ij} are the deviatoric stress components. The shape coefficients of Hill's quadratic yield function can be fitted from experimentally obtained mechanical data such as the

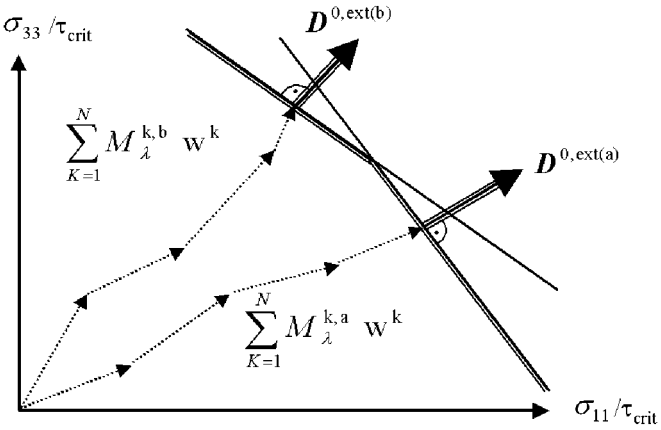

Fig. 6. The Taylor stress state for a polycrystalline aggregate can for a given external strain rate state be integrated as a volume weighted sum of all Taylor factors derived separately for each grain for the respective boundary condition. In this figure M is the Taylor tensor, D the strain rate and w the volume fraction. The counter k sums over all crystals in the aggregate.

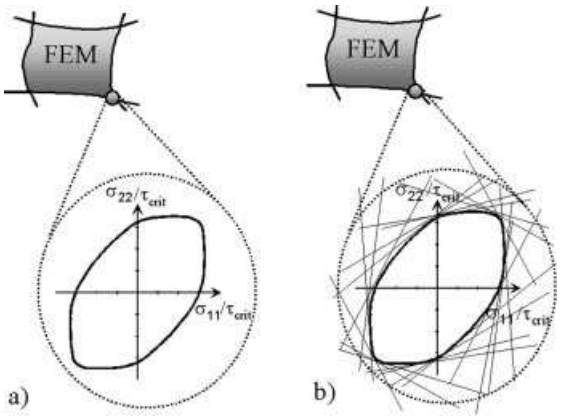

Fig. 7. Schematical presentation of an empirical (a) and of a texture-based (b) yield surface approach. It must be noted though that the actual incorporation of a crystallographic yield surface also requires a functional form.

Lankfort values taken in different directions of a specimen. Scaling can be provided by the yield stress obtained from uniaxial tensile testing. While the Lankfort coefficients and the yield stress can be determined from tensile testing, the direct measurement of mechanical response under complex loads is an intricate task. Although Hill-based anisotropy simulations (referring to the Hill 1948 model) provide decent approximations at least of the initial plastic anisotropy in case of certain iron textures and a number of textures in interstitial free steels, they typically fail to predict the yield shape of high strength steels, austenitic steels, most aluminum alloys, copper, or hexagonal materials. Typical examples where the Hill 1948 yield criterion is not applicable are cup drawing operations of aluminum or copper crystals with six-fold slip symmetry, i.e., with a crystal {111} plane parallel to the sheet surface (see paper by Roters and Zhao in this volume). In this case six slip systems have identical Schmid factor relative to the surface which cannot be modeled by the Hill polynomial owing to its quadratic form.

Due to this principle shortcoming a number of optimized empirical anisotropic yield surface concepts with higher order polynomial forms have been proposed in the last decades, such as those introduced later by Hill[3] and by Barlat[4] which are better suited for face centered cubic alloys and many body centered cubic steels. In the last years various authors have presented improved empirical yield surface approaches where the yield function can be fitted using both mechanically obtained and even texture-based data.

The chief advantage of using an empirical anisotropic yield surface function as a constitutive law in metal forming finite element simulations is time efficiency and the simple mechanical methods with which it can be derived. The dominant disadvantage of empirical yield surface functions is that the anisotropy of polycrystalline matter generally changes during forming owing to the change of texture. This evolution of anisotropy is not mapped by a corresponding change of the shape of the yield surface. In other words, the same yield surface shape is used throughout one finite element simulation without making a physically meaningful update of its steadily changing shape. Although empirical constitutive laws can be used to gradually change the yield surface shape during forming, their capability is typically constrained by a lack of physical information about the actual development of the crystallographic texture during forming.

5. Crystallographic Approximations of Elastic-Plastic Anisotropy

5.1. Crystallographic Approximations of Elastic Anisotropy Derived by Homogenization Theory

A typical problem in the field of anisotropy engineering is the approximation of the integral elastic response of a polycrystalline sample under an external load. Although various aspects can principally contribute to the anisotropy of the overall elastic stiffness we concentrate in the following on the influence of the crystallographic texture. The macroscopic elastic properties of a textured polycrystal can be calculated by formulating appropriate volume-weighted means of the individual elastic single crystal tensor, rotated parallel to the respective local coordinate system of each individual crystal. This average value of the integral elastic tensor must therefore take into account all individual orientations of the grains which are described by the orientation distribution function.

An early homogenization approach for the elastic response under an external load was suggested by Voigt, who assumed that in the case of a macroscopically prescribed strain rate state each material portion is in the same strain rate state as the entire sample, irrespective of its spatial position in the specimen. The strain rate would then be homogeneous throughout the sample. However, in a polycrystalline sample, the elastic response typically varies from grain to grain, due to the spatially changing crystal orientation. Since in the Voigt model the prescribed strain rate is the same everywhere in the sample, the stress must vary. The Voigt limit for the elastic response of a polycrystalline sample can thus be calculated by weighting the tensor of the elastic stiffness as a function of orientation with the orientation distribution function. A different approach to treating the homogenization problem in an elastically loaded polycrystalline sample was suggested by Reuss. He suggested that in the case of a macroscopically prescribed stress state each material portion is in the same stress state irrespective of its spatial position in the specimen. The stress would then be homogeneous throughout the specimen. The elastic response may then vary from grain to grain, in accord with the local orientation of the crystal. Since in the Reuss model the prescribed external stress is constant throughout the specimen, the strain must vary according to the local grain orientation. Consequently, the elastic Reuss limit can be calculated for a polycrystal by weighting the tensor of the elastic compliance as a function of orientation

with the orientation distribution function. Since neither the Voigt nor the Reuss method provides reliable approximations to the elastic modulus of a polycrystal, Hill defined an average modulus which consists of the equally weighted results of both above models.

5.2. Crystallographic Approximations of the Yield Surface Derived by Homogenization Theory

Polycrystalline alloys subject to metal forming operations typically develop or inherit morphological textures (e.g., elongated grains, chemical segregation, or second phases with elongated topology entailing directional effects) as well as crystallographic textures (orientation distribution of the crystallites constituting polycrystalline matter). While the former are often less relevant in typical commercial sheet material, the latter strongly determine the overall anisotropy. In the following we will hence concentrate on texture effects on yield anisotropy. Orientation distributions can directly serve as input data for the calculation of the crystallographically determined portion of the yield surface shape using Taylor-Bishop-Hill or self-consistent type approaches (Figs. 3, 7b). This applies for a single crystal yield surface as well as for the homogenization bounds of the polycrystal yield surface (Fig. 8). The major spirit and advantage of the crystallographic yield surface over empirical concepts consists in the fact that it reduces the individual anisotropic behavior of large sets of individual grains comprising a polycrystalline aggregate (10^4-10^{10} grains for a typical large scale forming operation) to a simple crystallographic homogenized shape function. It is thus an ideal example of a scale-bridging simulation approach which reduces the tremendous complexity inherent in real microstructures (Fig. 9) to a simple anisotropic function (Fig. 10).

Details about deriving the yield surface from the crystallographic texture of polycrystals are given in [5–11]. The required experimental input textures can be determined using x-ray, neutron, or electron diffraction experiments. Since texture-based yield surface approximations use the complete crystallographic anisotropy information of a specimen they are often superior to empirical approaches which rely on a small set of mechanical parameters. However, modern empirical approaches for the approximation of the yield surface typically use Taylor-Bishop-Hill type crystal simulations on the basis of experimental texture data to provide tangents for a better fit of the yield surface functions. Figure 11 shows the anisotropic effect of some isolated texture components in body centered cubic steels. The {111}<112> and the {111}<110> texture components each reveal a six-fold symmetry of the shape change with respect to the sheet surface, due to the symmetry of the active Burgers vectors and slip planes. In case that a complete fiber texture exists with a crystal <111> axis parallel to the sheet surface common to all orientations in that sample a very high r-value and a vanishing Δr-value are the consequence. A texture component which is very detrimental to the overall planar anisotropy for instance in ferritic steels is the cube orientation rotated 45° about the normal direction, {001}<110>. This texture component is often inherited from ferritic hot rolling steps and further sharpened during subsequent cold rolling of many low-carbon steels, most transformer steels, nearly all ferritic stainless steels, and all body centered cubic refractory metals such as molybdenum, tantalum, or niobium. Simulations of this kind would be essential for methods of inverse anisotropy engineering, where one first

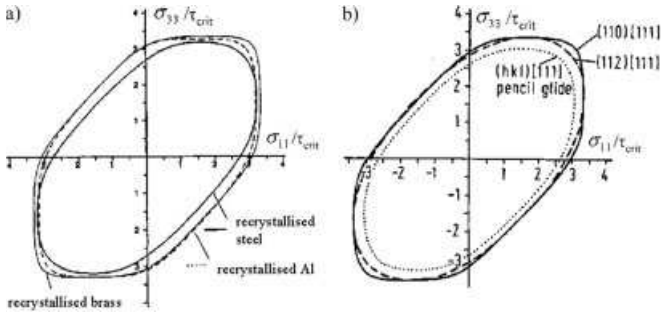

Fig. 8. Some examples of yield functions for different materials calculated by use of the homogenization bounds for their respective polycrystal yield surface. Figure (a) shows yield surface sections for aluminum, steel, and brass. Figure (b) shows yield surface sections for steel using different slip system combinations.

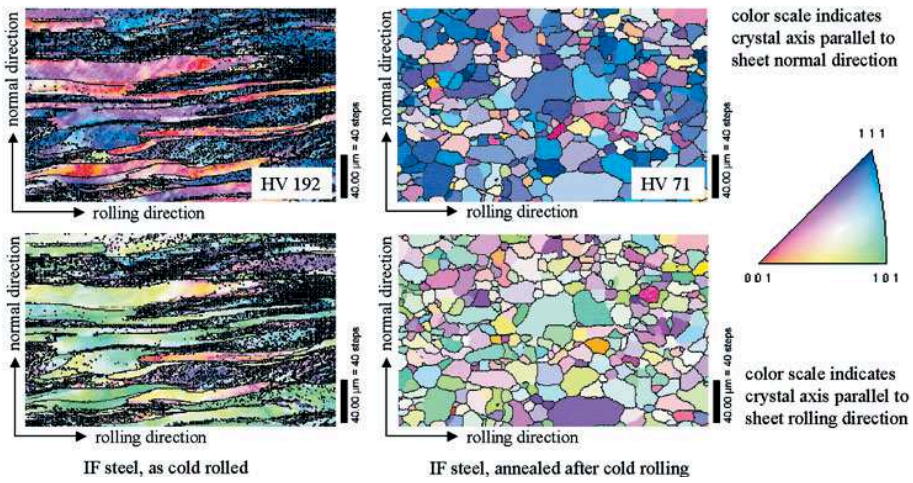

Fig. 9. Real microstructures (here an IF steel) reveal a tremendous complexity not only of the global but also of the local textures. This example shows that the incorporation of textures into finite element formulations requires adequate homogenisation approaches. The upper diagram shows a color scale which indicates the crystal axis parallel to sheet normal direction. The lower graph shows the crystal axis parallel to sheet rolling direction.

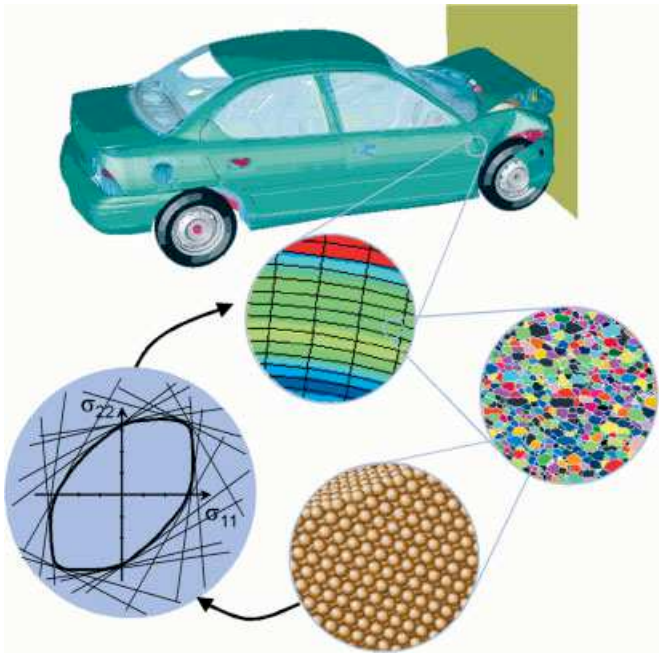

Fig. 10. The overview diagram shows the basic spirit of reducing microstructure complexity into a compact but at the same time physically based crystallographic yield formulation for including anisotropic behavior in metal forming simulations.

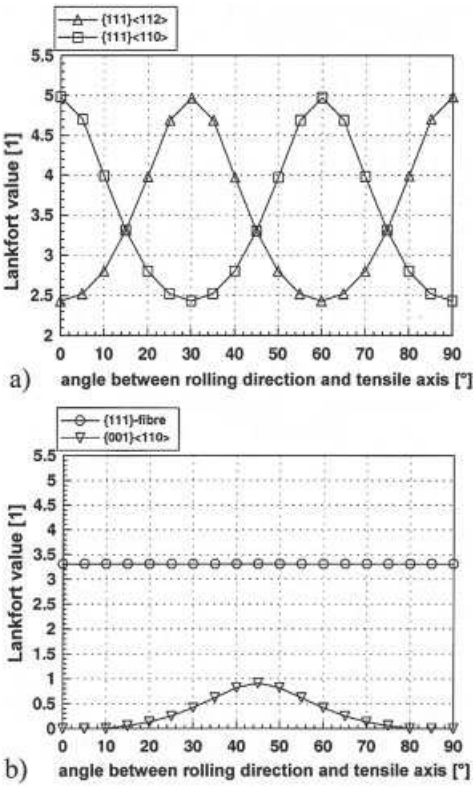

Fig. 11. Anisotropy of some isolated texture components in body centered cubic matter. The {111}<112> and the {111}<110> texture components each reveal a six-fold symmetry of the shape change with respect to the sheet surface, due to the symmetry of the active Burgers vectors and slip planes. In case of a complete <111> texture fiber with respect to the sheet surface a very high r-value and a vanishing Δr-value is the consequence. A very detrimental texture component is the cube orientation rotated 45° about the normal axis, {001}<110>.

identifies those texture components which are most beneficial for a given forming operation (this is not always necessarily a texture which creates a maximum r-value) and subsequently develops processing methods to generate this particular desired texture.

Besides its clear physical basis another advantage of crystallographic yield surface approximations lies in its capability to incorporate both, kinematical and kinetic plasticity effects. In this context it must be considered that the crystallographic texture only gives the respective anisotropic shape function for a particular polycrystalline sample, but the texture dependence of the internal stress and the individual hardness of the different grains are typically ignored by the constitutive laws employed in homogenisation approaches. However, it is principally feasible to generalize the crystallographic yield surface concept by enriching it with the individual strength of each grain. This leads to a formulation of the following kind

$$f(S_{ij}) = \frac{1}{V}\int_V M_{ij}\left(\boldsymbol{g}, D_{ij}\right)\ \tau_{\text{crit}}\left(D_{ij}, \boldsymbol{g}\right)\ \mathrm{d}V \approx \sum_{k=1}^{N} M_{ij}^{k}\ \tau_{\text{crit}}^{k}\ \ \mathrm{w}^{k} \tag{12}$$

where $f(S_{ij})$ is the yield surface, V the sample volume, M_{ij} the Taylor shape function obtained by homogenization theory as a function of strain rate D_{ij} and rotation matrix $\mathbf{g}$, τ_{crit} the flow stress of each individual grain, and w the volume fraction of each grain. An example where kinetic information about the local texture-dependent hardness of the various grains has been used to approximate a yield surface is given in Figure 12.[12] The left diagram shows a portion of the planar yield surface as it anisotropically shrinks during partial recrystallization. The right hand side of Figure 12 shows three subsequent time steps of a coupled crystal plasticity FEM - cellular automaton simulation where the upper picture gives the texture in terms of the magnitude of the Rodriguez vector and the lower picture the strength in terms of the dislocation density (black areas are recrystallized). The data from this discrete simulation served as input to the kinematic-kinetic yield surface model.

Although texture-based yield surface approximations have a crisp physical basis in that they incorporate crystal anisotropy in a genuine fashion, they have the shortcoming of ignoring texture changes during forming. This means that – as far as texture update during forming is concerned – there is basically little difference between the predictive capabilities of empirical and texture-based yield surface approximations, particularly if one considers that recent approaches use both, mechanical and texture-related information to fit the yield function. These methods could be referred to as hybrid anisotropy yield criteria or semi-empirical yield criteria.

ADVANCED ENGINEERING MATERIALS

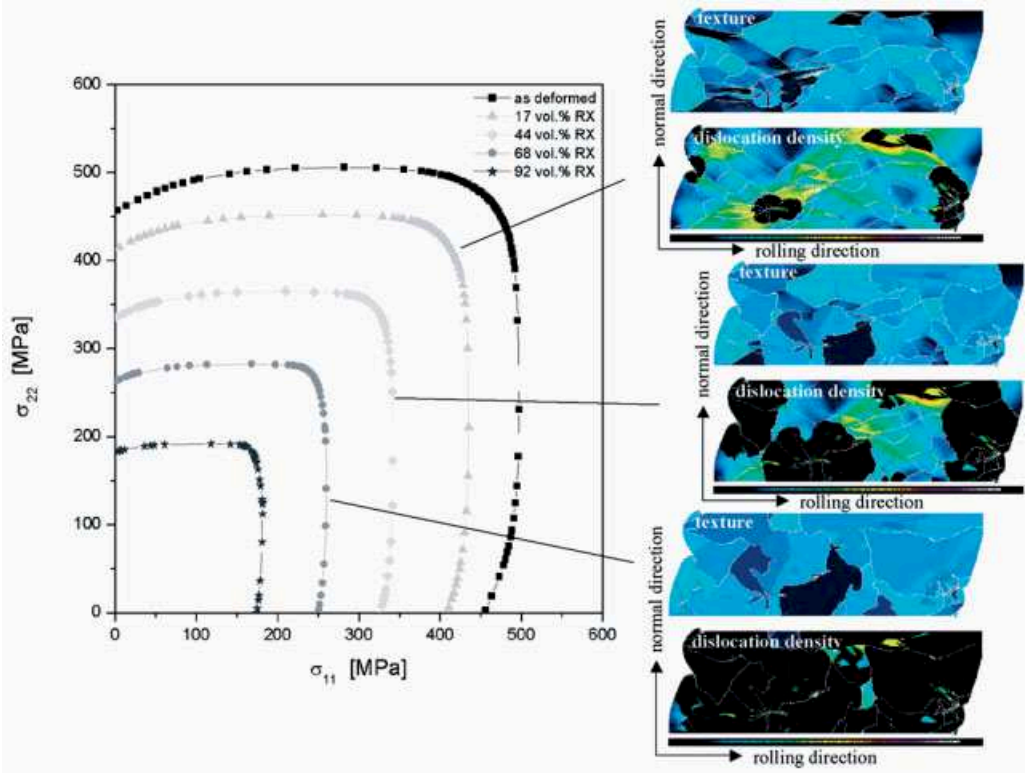

Fig. 12. Coupled crystallographic-kinetic yield functions obtained by including both the texture and the texture dependent flow stress of each individual grain weighted by it respective volume [12]. The left hand side of the diagram shows a portion of the planar yield surface as it anisotropically shrinks during partial recrystallization. The right hand side shows three subsequent time steps of a coupled crystal plasticity FEM - cellular automaton simulation where the upper picture gives the texture in terms of the magnitude of the Rodriguez vector and the lower picture the strength in terms of the dislocation density.

6. Integration of Continuum and Crystal Plasticity Homogenization Models

Recent methods for the approximation of plastic anisotropy aim at combining Taylor-based texture homogenization models with isotropic non-linear finite element simulations.[13,14] In this approach the deformation tensor after each strain increment is used to prescribe the boundary conditions for a corresponding Taylor simulation using a full constraints or coupled full constraints/grain interaction strain rate homogenization model. Each of the finite elements contains its representative crystallographic texture information in the form of a discrete set of grain orientations. The Taylor factor calculated from homogenization is fed back into the finite element simulation as a correction factor for the flow stress in the ensuing simulation step.

The particular strength of this method lies in the realistic simulation of texture changes under complex boundary conditions. With respect to large scale engineering applications a shortcoming of the approach lies in the fact that a large number of discrete orientations is required for a mathematically correct representation of the texture. This entails long computation times when simulating metal forming operations with complete texture update.

7. Crystal Plasticity Finite Element Simulation

A direct integration of crystal plasticity phenomena into non-linear variational formulations was first suggested by Peirce, Needlemann and Asaro.[15,16] Based on these approaches implicit integration schemes which were for instance developed by Becker[17] and Kalidindi[18] are designed in a way which allows one to directly implement them in the form of user-defined subroutines into commercial finite element software packages. The current approaches in this domain provide a direct means for updating the local crystallographic and hardening state of the material via integration of the evolution equations for the crystal lattice orientation and the critical resolved shear stress. The deformation behavior of the crystal volume elements are at each integration point governed by a crystal plasticity model which accounts for discrete plastic deformation by crystallographic slip and for the rotation of the crystal lattice during deformation (Fig. 13). The crystal plasticity finite element models typically use space and time as independent variables and the crystal orientation and the accumulated slip as dependent variable.

In the large-strain constitutive crystal model modified for the present work one assumes the stress response at each macroscopic continuum material point to be poten-

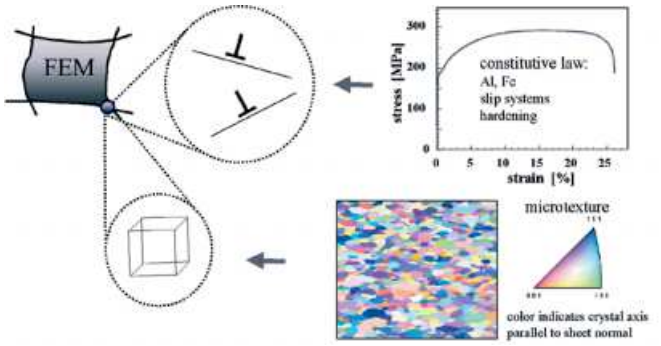

Fig. 13. Schematical presentation of a crystal plasticity finite element formulation for considering and predicting texture-based plastic anisotropy on a grain-for-grain scale.

tially given by one crystal or by a volume-averaged response of a set of grains comprising the respective material point. In case of a multi-grain description the volume averaged stress amounts to

$$\langle \mathbf{T} \rangle = \sum_{k=1}^{N} \left(w_k \mathbf{T}_k \right) \tag{13}$$

where N is the number of grains at each integration point, w_k the volume fraction of each crystal, and T_k the Cauchy stress in the kth crystal. The constitutive equation for the stress in each grain is then expressed in terms of

$$\mathbf{T}^* = \mathbf{C}\mathbf{E}^* \tag{14}$$

where **C** is the fourth order elastic tensor and **E*** an elastic strain measure obtained by polar decomposition,

$$\mathbf{E}^* = \frac{1}{2}\left(\mathbf{F}^{*\mathrm{T}}\,\mathbf{F}^* - \mathbf{1} \right) \tag{15}$$

which leads to a stress measure which is the elastic work conjugate to the strain measure **E***,

$$\mathbf{T}^* = \mathbf{F}^{*-1}\left(\det\left(\mathbf{F}^*\right)\mathbf{T} \right)\mathbf{F}^{*-T} \tag{16}$$

where T is the symmetric Cauchy stress tensor in the grain, and **F*** is a local elastic deformation gradient defined in terms of the local *total* deformation gradient **F** and the local *plastic* deformation gradient $\mathbf{F}^p$. The relation between the elastic and the plastic portion of **F** amounts to

$$\mathbf{F}^* = \mathbf{F}\,\mathbf{F}^{p-1}, \quad \det(\mathbf{F}^*) > 0, \quad \det(\mathbf{F}^p) = 1 \tag{17}$$

The plastic deformation gradient is given by the flow rule

$$\dot{\mathbf{F}}^p = \mathbf{L}^p\,\mathbf{F}^p \tag{18}$$

with its crystalline portion

$$\mathbf{L}^p = \sum_{k=1}^{N} \dot{\gamma}_k\, \mathrm{m}_k,\ \dot{\gamma}_k = f(\tau_k, \tau_{k,\mathrm{crit}}),\ \tau_k \approx \mathbf{L}^* \cdot \mathrm{m}_{k,0} \tag{19}$$

where m_k are the k dyadic slip products introduced above, γ_k the shear rates on these systems, and $\tau_{k,\mathrm{crit}}$ the actual critical shear stress on the *kth* system. For room temperature simulations of aluminum plastic deformation is commonly assumed to occur on the 12 slip systems with ⟨110⟩ slip directions and {111} slip planes, i.e., the slip vectors $b_i = {}^1/_{\sqrt{2}}\,(110)$ and $n_i = {}^1/_{\sqrt{3}}\,(111)$ are orthonormal. For room temperature simulations of iron plastic deformation can be assumed to occur on 12 $b_i = {}^1/_{\sqrt{3}}\,(111)$, $n_i = {}^1/_{\sqrt{2}}\,(110)$ systems, 12 $b_i = {}^1/_{\sqrt{3}}\,(111)$, $n_i = {}^1/_{\sqrt{6}}\,(112)$; systems, and 24 $b_i = {}^1/_{\sqrt{3}}\,(111)$, $n_i = {}^1/_{\sqrt{14}}\,(123)$ systems.

For many simulations in this field, the strengths of all slip systems at a material point are taken to be equal, i.e., one adopts the Taylor hardening assumption. The hardening as a function of total slip can be assumed to follow experimentally observed or theoretically achieved macroscopic strain hardening behavior obtained from a uniaxial or biaxial test by fitting the experimental data to a standard scalar constitutive equation. The fit can be adjusted by the average Taylor factor of the sample and its change during deformation to give the slip system threshold stress as a function of the accumulated shear. Most of the results presented in this work have been achieved by accounting for latent hardening through the use of an appropriate hardening matrix.

Crystal plasticity finite element models represent elegant tools for detailed joint simulation studies of texture evolution and strain distribution under realistic boundary conditions (Fig. 14). Each integration point can represent one single orientation or map even a larger set of crystals. Although the latter case is principally feasible, it entails long calculation times, rendering the method less practicable for industry-scale applications.

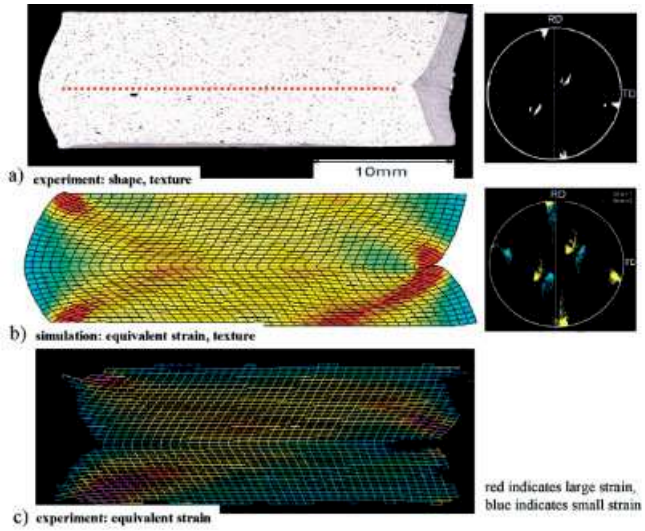

Fig. 14. Example where a grain-for-grain crystal plasticity finite element model was applied for a joint simulation study of texture and strain under realistic boundary conditions. The example shows the deformation of an aluminum bicrystal. The upper diagram shows the shape change of the two grains and the experimentally determined microtexture. The mid section shows the von Mises strain distribution and the microtexture predicted by a corresponding crystal plasticity finite element simulation. The lower graph gives the experimentally determined strain distribution.

ADVANCED ENGINEERING MATERIALS

8. Integrating Texture Components into the Crystal Plasticity Finite Element Method

A novel physically based and highly time efficient approach for including and updating texture-based elastic-plastic anisotropy during large-strain metal forming operations lies in the integration of crystallographic texture components into the crystal plasticity finite element method.[19,20] The approach is particularly designed for industrial use since it can be assembled by integrating existing software solutions from crystallography and variational mathematics. The approach is based on directly feeding spherical crystallographic texture components into a non-linear finite element model (Fig 15). The method is used for performing fast simulations of industry-scale metal forming operations of textured polycrystalline materials including texture update. Instead of yield surface concepts or large sets of discrete grain orientations it uses a small set of discrete and mathematically compact Gaussian texture components to map the orientation distribution discretely onto the integration points of a viscoplastic crystal plasticity finite element model. This method drastically enhances the computing speed and precision compared to previous large scale - large strain crystal plasticity finite element approaches.

The texture component method used for this approach is based on the introduction of symmetrical spherical Gauss or Bessel-Gauss functions for the approximation of the orientation distribution.[21,22] This method provides a small set of compact texture components which are characterized by simple parameters of physical significance (three Euler angles, full width at half maximum, volume fraction). Using this method, only a few texture components are required for mapping the complete texture in a mathematical precise form. As starting data one can use both, statistical textures taken from neutron and x-ray measurements or microtextures determined via electron diffraction in the SEM or TEM (Fig. 15). The advantages of this novel approach are at hand. First, one can simulate metal forming operations with complete consideration of elastic-plastic anisotropy and gradual local texture update at the same time (Fig. 16). Second, one can within reasonable computation times quantitatively investigate the texture changes that take place during metal forming (Fig. 17). This information can help to better select which anisotropy concept is appropriate for the different kinds of metal forming boundary conditions and materials. For instance, in cases where only small texture changes take place it can be useful - due to simulation speed - to use one of the conventional yield surface concepts which neglect texture update.

9. Quintessence

The article presented different empirical and physically based concepts for the integration of the elastic-plastic anisotropy of polycrystalline matter into both, small scale and large scale metal forming finite element simulations. The reviewed anisotropy concepts were empirical yield surface approximations, texture-based yield surface formulations based on crystallographic homogenization theory, combinations of finite element and texture-based polycrystal homogenization approaches, the crystal plasticity finite element method, and the recently introduced texture component crystal plasticity finite element method. The article presented the basic physical approaches behind the different methods and reviewed

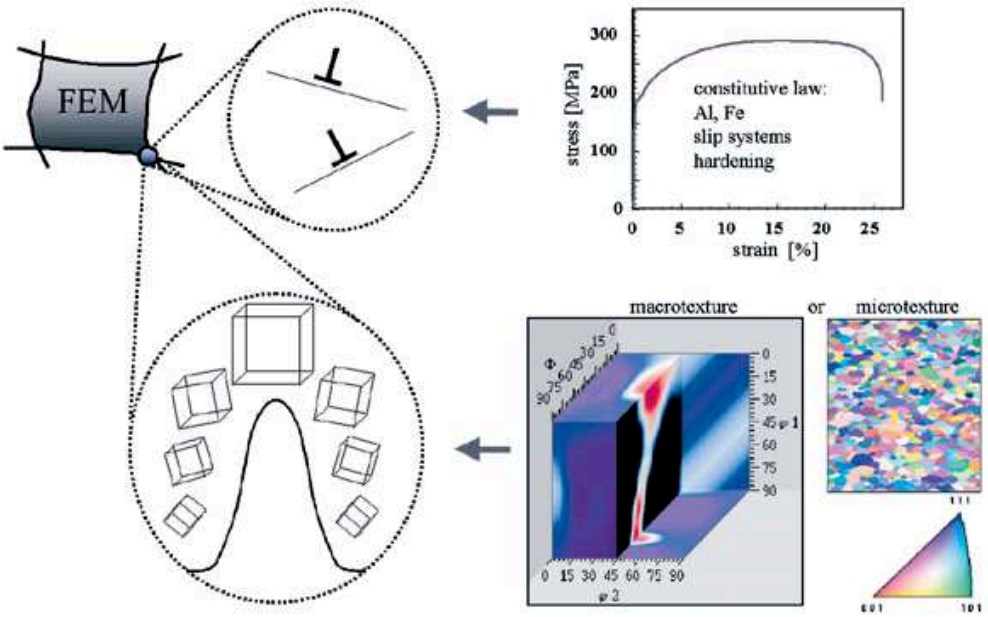

Fig. 15. Schematical presentation of a new physically based and time efficient approach for including and updating texture-based elastic-plastic anisotropy during large-strain metal forming operations [19,20]. The method integrates crystallographic texture components into the crystal plasticity finite element method and is hence referred to as texture component crystal plasticity finite element method (TCCP-FEM). It can make use of both, microtextures or statistical texture information.

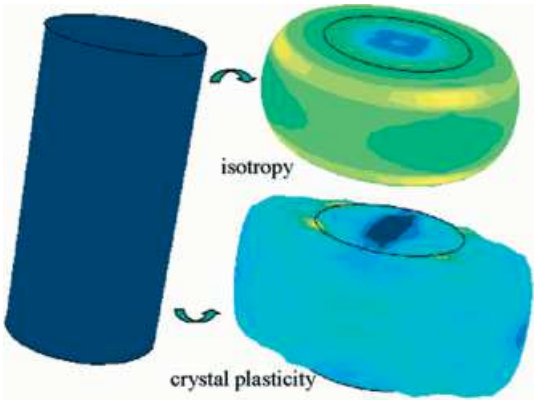

Fig. 16. Example of an isotropic and an anisotropic compression test simulation.

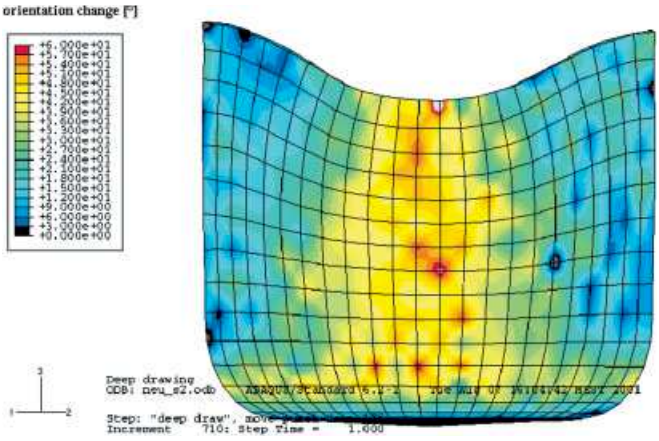

Fig. 17. The texture component crystal plasticity finite element method allows one to quantitatively investigate within reasonable calculation times the texture changes that take place during metal forming. This information is important to select which anisotropy concept is appropriate for the different kinds of metal forming boundary conditions and materials. For instance, in cases where only small texture changes take place it can be useful - due to simulation speed - to use one of the conventional yield surface concepts which neglect texture update.

various engineering aspects such as scalability, flexibility, and texture update in the course of a forming or crash simulation. The present state of the art in anisotropy engineering is naturally different between the day-to-day industry practice and basic science. The use of empirical or semi-empirical higher-order polynomial approximations of the yield surface is a quasi standard operation with respect to industrial applications whereas the various crystal plasticity finite element methods increasingly gain prevalence as a quasi standard in the basic materials sciences. The dominance of empirical approaches in the industrial practice is due to the fact that they provide short computation times, allow for simple mechanical input data, and are flexible with respect to additional fit points obtained by texture information. The major drawback of empirical approaches is the absence of texture and anisotropy update. The dominance of the crystal plasticity finite element method in the basic sciences is due to its sound physical basis and the complete incorporation of texture and anisotropy update. The major disadvantage of these approaches are the long calculation times which presently exceed those obtained by use of the yield surface roughly by a factor of 50–100. An improvement in speed of the crystal plasticity formulations is attained by the recent introduction of the texture component crystal plasticity finite element method which differs from the speed of yield surface calculations only by a factor of 15–25.

Received: December 21, 2001

[1] R. V. von Mises, *Zeitschr. Angew. Math. Mech.*, **1928,** *8*, 161.
[2] R. Hill, *Proc. Royal Society* **1948**, 193, 281.
[3] R. Hill, *Mech. Phys. Solids* **1990**, *38*, 405.
[4] F. Barlat, J. Lian, *Intern. J. Plasticity*, **1989**, *5*, 51.
[5] W. F. Hosford, *The Mechanics of Crystals and Textured Polycrystals*, Oxford University Press **1993**.
[6] U. F. Kocks, C. N. Tóme, H.-R. Wenk, *Texture and Anisotropy*, Cambridge University Press **1998**.
[7] H.- J. Bunge, *Kristall u.Technik* (in German) **1970**, 5, 145.
[8] P. Van Houtte, K. Mols, B. Van Bael, E. Aernoudt, *Texture and Microstructures*, **1989**, *11*, 23.
[9] A. Van Bael, P. Van Houtte, E. Aernoudt, F. R. Hall, L. Pillinger, P. Hartley, C. E. N. Sturgess, *J. Text. Microstruct.*, **1991**, *14–18*, 1007.
[10] D. Raabe, *Computational Materials Science*, Wiley-VCH, Weinheim **1998**.
[11] D. Raabe, *Comp. Mater. Sci.*, **2000**, *19*, 13.
[12] K. Berner, B. Engl, U. Müller, V. Steininger, E. Till, *Stahl u. Eisen*, **1996**, *116*, 52.
[13] H. Aretz, R. Luce, M. Wolske, R. Kopp, M. Goerdeler, V. Marx, G. Pomana, G. Gottstein, *Modell. Simul. Mater. Sci. Eng.*, **2000**, *8*, 881.
[14] B. Beckers, G. Pomana, G. Gottstein, in *Proceedings of Conference on Constitutive and Damage Modeling of Inelastic Deformation and Phase Transformations*, A. S. Khan (Ed.), Neat Press, Fulton, Maryland, USA, **1998,** p. 305.
[15] D. Piece, R. J. Asaro, A. Needleman, *Acta Metall.*, **1982**, *30*, 1087.
[16] R. J. Asaro, *Adv. Appl. Mech.*, **1983**, *23*, 1.
[17] R. C. Becker, *Acta Metall. Mater.*, **1991**, *39*, 1211.
[18] S. R. Kalidindi, C. A. Brounkhorst, L. J. Anand, *Mech. Phys. Solids*, **1991**, *40*, 537.
[19] Z. Zhao, F. Roters, W. Mao, D. Raabe, *Adv. Eng. Mater.* **2001**, *3*, 984.
[20] D. Raabe, Z. Zhao, F. Roters, *Steel Research*, **2001**, *72*, 421.
[21] K. Lücke, J. Pospiech, K. H. Virnich, J. Jura, *Acta Metall.*, **1981**, *29*, 167.
[22] K. Helming, R. A. Schwarzer, B. Rauschenbach, S. Geier, B. Leiss, H. Wenk, K. Ullemeier, J. Heinitz, *Z. Metallkd.*, **1994,** *85***,** 545.